HHS Public Access

Author manuscript

Methods Enzymol. Author manuscript; available in PMC 2020 January 03.

Published in final edited form as:

Methods Enzymol. 2013 ; 526: 145–157. doi:10.1016/B978-0-12-405883-5.00009-0.

Real-Time Monitoring of Reactive Oxygen and Nitrogen Species in a Multiwell Plate Using the Diagnostic Marker Products of Specific Probes

Jacek Zielonka[*], **Joy Joseph**[*], **Adam Sikora**[*,†], **Balaraman Kalyanaraman**[*,1]

[*] Department of Biophysics and Free Radical Research Center, Medical College of Wisconsin, Milwaukee, Wisconsin, USA [†] Institute of Applied Radiation Chemistry, Lodz University of Technology, Lodz, Poland

Abstract

Developing rigorous assays for cellular detection of reactive oxygen and nitrogen species ($O_2^{\cdot-}$, H_2O_2, $^{\cdot}NO$, and $ONOO^-$) is an active area of research in our laboratory. Published reports suggest that diagnostic marker products are formed as a result of interaction of these species with small molecular weight fluorescent and nonfluorescent probes. In this chapter, we describe an HPLC-based methodology to detect formation of these species in biological and cellular systems. By monitoring the diagnostic marker products formed from reaction between specific chemical probes and the oxidant species, it is possible to simultaneously assay these species using a multiwell plate (e.g., 384-well plate).

1. INTRODUCTION

The purpose of this article is to demonstrate the feasibility of using a diagnostic marker-based high-throughput methodology for detecting reactive oxygen and nitrogen species (ROS/RNS) [e.g., superoxide (O_2-), hydrogen peroxide (H_2O_2), nitric oxide ($^{\cdot}NO$), peroxynitrite ($ONOO^-$)] in a multiwell (96-well, 384-well) plate format. The main methodology to be used is HPLC or UHPLC with absorption and fluorescence detection or in combination with mass spectrometry. The chemical probes to be used are hydroethidine (HE) for $O_2^{\cdot-}$, coumarin boronate (CBA) for H_2O_2 and $ONOO^-$, diaminofluorescein (DAF-2) for $^{\cdot}NO$, and *ortho*-triphenylphosphonium-substituted phenylboronate [*o*-Mito-PhB$(OH)_2$] for specific detection of $ONOO^-$. The structures of the probes and diagnostic marker products derived from them as a result of interaction with specific ROS/RNS are shown in Fig. 9.1. Previously, we described a similar experimental design in which the initial screening of these species was performed using fluorescent probes (HE, CBA, DAF-2, and Amplex Red) in a 96-well plate by real-time monitoring increase in fluorescence intensity using a plate reader (Zielonka, Sikora, Hardy, Joseph, Dranka, & Kalyanaraman, 2012; Zielonka, Zielonka et al., 2012). We recommended the use of HPLC-based analyses to

[1] Corresponding author: balarama@mcw.edu.

further confirm and rigorously identify the specific products formed from the fluorogenic probes.

Recently, significant advances have been made with regard to reaction mechanisms (rate constants, stoichiometry, and product characterization) of $O_2^{\cdot-}$, H_2O_2, $ONOO^-$, and $^{\cdot}NO$ with fluorogenic dyes that have infused increased confidence, rigor, and reliability in ROS/RNS assays (Michalski, Zielonka, Hardy, Joseph, & Kalyanaraman, 2013; Robinson et al., 2006; Sikora et al., 2011; Sikora, Zielonka, Lopez, Joseph, & Kalyanaraman, 2009; Zhao et al., 2005, 2003; Zielonka, Sikora, et al., 2012; Zielonka, Vasquez-Vivar, & Kalyanaraman, 2008; Zielonka, Zielonka, et al., 2012). For example, the long-held notion that $O_2^{\cdot-}$ reacts with HE to form ethidium (E^+) has been debunked; instead, the only major product of the reaction between HE and $O_2^{\cdot-}$ was identified as 2-hydroxyethidium (2-OH-E^+) (Zhao et al., 2003, 2005). Other oxidants ($ONOO^-$-derived oxidants including OH, and higher oxidants derived from peroxidases) react with HE to form other oxidation products (E^+, and dimeric products), all of which can be readily separated and identified by HPLC and mass spectrometry (Zhao et al., 2005; Zielonka, Srinivasan, et al., 2008; Zielonka, Vasquez-Vivar, et al., 2008). These studies have exposed and highlighted the pitfalls and limitations of fluorescence microscopy in assessing intracellular and mitochondrial $O_2^{\cdot-}$ (Kalyanaraman, Dranka, Hardy, Michalski, & Zielonka, in press; Zielonka & Kalyanaraman, 2010). The discovery of a rapid, direct, and nearly stoichiometric reaction between $ONOO^-$ and boronates forming specific products has enabled the differentiation between $ONOO^-$ and myeloperoxidase/H_2O_2/NO^--based nitration mechanisms (Sikora et al., 2011, 2009; Zielonka, Sikora, et al., 2012; Zielonka, Zielonka, et al., 2012). Kinetic analyses of boronate reactions with H_2O_2 and $ONOO^-$ have made it possible to clearly and distinctly interpret the data in enzymatic and cellular systems cogenerating these species (Sikora et al., 2011, 2009; Zielonka, Sikora, et al., 2012; Zielonka, Sikora, Joseph, & Kalyanaraman, 2010; Zielonka, Zielonka, et al., 2012).

Whereas the initial screening in a fluorescence plate reader followed by a rigorous HPLC characterization may be a useful approach in a high-throughput screening of several thousands of compounds from chemical libraries, the HPLC/MS detection and identification of diagnostic marker products of ROS/RNS-specific probes are most critical for elucidating the chemical, biological, and signaling pathways in cells. In this chapter, we describe the use of four different chemical probes specific for monitoring $O_2^{\cdot-}$, H_2O_2, $^{\cdot}NO$, and $ONOO^-$ formation in cell-free and cell systems.

2. EXPERIMENTAL METHODS

2.1. Assay plate layout

Prior to using the global profiling approach in cellular systems, the uninitiated investigators should become familiar with the assay using xanthine (X) or hypoxanthine (HX)/xanthine oxidase (XO) as a source of superoxide flux and the $^{\cdot}NO$ donor, DPTA-NONOate, that decomposes to slowly release $^{\cdot}NO$ (Fig. 9.2A). Defined fluxes of $O_2^{\cdot-}$and $^{\cdot}NO$ are simultaneously generated from X (or HX)/XO and DPTA-NONOate in a 96-well plate (Fig. 9.2B). The proposed experimental approach for HPLC (or UHPLC)-based monitoring of ROS/RNS using the four different probes is shown in Fig. 9.3. HPLC conditions for fast

analyses of the probes and their products have been described in earlier publications (Sikora et al., in press; Zielonka, Sikora, et al., 2012; Zielonka, Zielonka, et al., 2012).

3. RESULTS AND DISCUSSION

3.1. HPLC analyses of HE-derived products

Figure 9.2B shows the "cell-free" assay setup in a 96-well plate containing HE in the presence of varying fluxes of $^{\cdot}NO$ and $O_2^{\cdot-}$ generated from HX/XO and DPTA-NONOate. Representative HPLC chromatograms (absorption and fluorescence) of HE metabolites are shown in Fig. 9.4A. Under conditions in which only $O_2^{\cdot-}$ and H_2O_2 were generated (right bottom corner well in Fig. 9.2B), the HPLC profile corresponds mainly to 2-OH-E^+, the diagnostic marker product of HE/$O_2^{\cdot-}$reaction and very little E^+ or dimers. Under conditions in which both $O_2^{\cdot-}$ and $^{\cdot}NO$ are maximally produced at a 1:1 ratio (top right corner well in Fig. 9.2B), 2-OH-E^+ was dramatically inhibited; instead, there was increased formation of E^+ and dimers (HE-E^+, E^+-E^+). Under other conditions, different levels of these products were formed. Indeed, a complete profile of 2-OH-E^+ formation under different fluxes of $^{\cdot}NO$ and $O_2^{\cdot-}$ has been reported (Zielonka, Zielonka, et al., 2012).

From these results, we conclude the following: (1) 2-OH-E^+, the specific marker product of HE reaction with $O_2^{\cdot-}$, increased with increasing $O_2^{\cdot-}$ flux and $^{\cdot}NO$ inhibited 2-OH-E^+ formation in a concentration-dependent fashion. (2) With increasing $^{\cdot}NO$ and $O_2^{\cdot-}$, the levels of E^+ and dimeric (e.g., E^+-E^+) products increased, suggesting the formation of one-electron oxidants ($^{\cdot}NO$ and O_2 and $ONOO^-$-derived oxidants). (3) Although the HPLC data show a marked decrease in 2-OH-E^+, the fluorescence intensity remained high due to increased levels ofE^+. Clearly, the measurements of HE oxidation-derived fluorescence cannot be equated to $O_2^{\cdot-}$ formation. The mechanism of formation of 2-OH-E^+ and E^+ is very different.

Once the investigators become conversant with the HPLC analyses in the well-defined "cell-free" model system, they will be able to perform studies in cellular systems. To investigate oxidation products of HE by endogenously generated $O_2^{\cdot-}$, $^{\cdot}NO$, and $ONOO^-$, we used a system consisting of RAW 264.7 macrophages stimulated with a mixture of LPS, IFN-γ, and PMA (Fig. 9.2C). Oxidation of HE was monitored in a 96-well plate and products formed in cells and in media were analyzed by HPLC. Macrophages were seeded in 96-well plates, and PMA, LPS, or IFN-γ were added as indicated in the presence of HE. The corresponding HPLC profiles are shown in Fig. 9.4B. As shown, 2-OH-E^+ formation increased in the presence of macrophages activated by PMA. Similar to the cell-free system, costimulation of $^{\cdot}NO$ and $O_2^{\cdot-}$ production during the combined treatment with IFN-γ, LPS, and PMA decreased the yield of 2-OH-E^+ with a concomitant increase in HE-derived dimeric products.

3.2. HPLC analyses of CBA-derived products

The "cell-free" assay setup is similar to conditions described in Fig. 9.2B but using coumarin boronic acid (CBA) probe (Fig. 9.1). Oxidation products of CBA were monitored under varying fluxes of $^{\cdot}NO$ and $O_2^{\cdot-}$. Representative HPLC chromatograms are shown in

Fig. 9.5A. As can be seen, there is very little oxidation of CBA to 7-hydroxycoumarin (COH) in the presence $^{\cdot}NO$ or $O_2^{\cdot-}$alone. However, there is a dramatic increase in the formation of COH in the presence of both $^{\cdot}NO$ and $O_2^{\cdot-}$. This is consistent with the very rapid reaction between $ONOO^-$ and CBA. CBA reacts with H_2O_2 stoichiometrically. However, because this reaction is rather slow, much higher concentrations (millimolar range) of CBA are needed to detect and quantitate H_2O_2. Thus, in the presence of $ONOO^-$, it is essential to measure catalase-inhibitable amount of COH in order to assess H_2O_2 formation. The reaction between CBA and H_2O_2 to form COH is catalase sensitive, whereas the $ONOO^-$/CBA reaction is catalase insensitive (Zielonka, Sikora, et al., 2012; Zielonka et al., 2010; Zielonka, Zielonka, et al., 2012). The oxidation of CBA by activated macrophages was monitored in a 96-well plate. Macrophages were stimulated with LPS, IFN-γ, and PMA, as described previously. Representative HPLC profiles are shown in Fig. 9.5B. Substantial oxidation of CBA to COH was observed in the presence of IFN-γ, LPS, and PMA. L-NAME significantly inhibited COH formation, as did SOD. These results suggest that CBA can be used to selectively detect ONOO− formed from macrophages activated to cogenerate $^{\cdot}NO$ and $O_2^{\cdot-}$.

3.3. HPLC analyses of DAF-2-derived products

The formation of a triazole, DAF-2T, formed from nitrosation of DAF-2 has been used to monitor intracellular $^{\cdot}NO$ formation (Thomas, Kotamraju, Zielonka, Harder, & Kalyanaraman, 2007). The “cell-free” assay setup is similar to experimental conditions described in Fig. 9.2B. Nitrosation of DAF-2 was monitored in a 96-well plate in the presence of cogenerated $^{\cdot}NO$ and $O_2^{\cdot-}$. $^{\cdot}NO$ alone induces formation of DAF-2T in the presence of oxygen or superoxide. Oxidation of DAF-2 may “activate” the probe to react with $^{\cdot}NO$ and thus increase the yield of DAF-2T. The representative HPLC traces are shown in Fig. 9.6. It is clear that $^{\cdot}NO$ is required to produce DAF-2T, both in cell-free and cellular systems. However, other factors may also affect the yield of the product, as exemplified by the amplifying effect of superoxide on the yield of DAF-2T in cell-free system (Fig. 9.6A). As shown previously, bell-shaped response of DAF-2 nitrosation to different superoxide fluxes indicates the possibility of both enhancement and inhibition of DAF-2T formation, depending on the actual ratio of superoxide and nitric oxide fluxes. Under the conditions of excess of superoxide, virtually all $^{\cdot}NO$ is scavenged and the yield of DAF-2T decreased. In this case, the decrease of DAF-2T formation may be therefore interpreted as a diminished bioavailability of “free” $^{\cdot}NO$, as exemplified in Fig. 9.6B.

3.4. HPLC analyses of *ortho*-Mito-PhB(OH)$_2$-derived products

The oxidative transformation of *o*-Mito-PhB$(OH)_2$ probe in the presence of peroxynitrite is shown in Fig. 9.7A. In contrast to other arylboronates, with *o*-Mito-PhB$(OH)_2$, the relative yield of the minor nitration product (*o*-Mito-PhNO_2) is independent of the presence of biologically relevant reductants (Sikora et al., in press). The ratio between *o*-Mito-PhNO_2 and *o*-Mito-PhOH during $ONOO^-$-dependent oxidation of *o*-Mito-PhB $(OH)_2$ remained constant. The actual yields of both products can be used to determine the contribution of different oxidants ($ONOO^-$ or H_2O_2) to oxidation of the probe. As *o*-Mito-PhNO_2 is not formed by H_2O_2 or HOCl or MPO/H_2O_2/NO_2^- system, it can be used as a specific diagnostic

marker of $ONOO^-$ (Sikora et al., in press). As shown in Fig. 9.7B, HPLC separation of different products can be achieved within 5 min, and the analysis time is expected to be significantly shortened with the use of UHPLC systems.

4. SUMMARY

The HPLC assays using ROS/RNS-specific chemical probes reported here with well-defined redox chemistry are simple yet rigorous and can readily be implemented in cell-based high-throughput studies (e.g., in 384- and 1536-well plates) using automated liquid-handling systems. Increased understanding of the free radical and non-free radical chemistry of fluorescent probes has exposed and highlighted the limitations of fluorescence microscopy-based ROS/RNS assays.

ACKNOWLEDGMENTS

This work was supported by funds received from NHLBI (R01 HL063119). A. S. was supported by a grant from the Foundation for Polish Science (FNP) within the “Homing Plus” program and a grant coordinated by JCET, No. POIG.01.01.02-00-069/09 (both grants are supported by the European Union from the resources of the European Regional Development Fund under the Innovative Economy Programme).

REFERENCES

Kalyanaraman B, Dranka BP, Hardy M,Michalski R, & Zielonka J (in press). HPLC-based monitoring of products formed from fluorogenic probes—The ultimate approach for intra-and extracellular superoxide detection. Biochimica et Biophysica Acta General Subjects. 10.1016/j.bbagen.2013.05.008.

Michalski R, Zielonka J, Hardy M, Joseph J, & Kalyanaraman B (2013). Hydropropidine: A novel, cell-impermeant fluorogenic probe for detecting extracellular superoxide. Free Radical Biology & Medicine, 43, 135–147.

Robinson KM, Janes MS, Pehar M, Monette JS, Ross MF, Hagen TM, et al. (2006). Selective fluorescent imaging of superoxide in vivo using ethidium-based probes. Proceedings of the National Academy of Sciences of the United States of America, 103, 15038–15043. [PubMed: 17015830]

Sikora A, Zielonka J, Adamus J, Debski D, Dybala-Defratyka A, Michalowski B, et al. (in press). Reaction between peroxynitrite and triphenylphosphonium-substituted arylboronic acid isomers—Identification of diagnostic marker products and biological implications. Chemical Research in Toxicology. 10.1021/tx300499c.

Sikora A, Zielonka J, Lopez M, Dybala-Defratyka A, Joseph J, Marcinek A, et al. (2011). Reaction between peroxynitrite and boronates: EPR spin-trapping, HPLC analyses, and quantum mechanical study of the free radical pathway. Chemical Research in Toxicology, 24, 687–697. [PubMed: 21434648]

Sikora A, Zielonka J, Lopez M, Joseph J, & Kalyanaraman B (2009). Direct oxidation of boronates by peroxynitrite: Mechanism and implications in fluorescence imaging of peroxynitrite. Free Radical Biology & Medicine, 47, 1401–1407. [PubMed: 19686842]

Thomas S, Kotamraju S, Zielonka J, Harder DR, & Kalyanaraman B (2007). Hydrogen peroxide induces nitric oxide and proteosome activity in endothelial cells: A bellshaped signaling response. Free Radical Biology & Medicine, 42, 1049–1061. [PubMed: 17349932]

Zhao H, Joseph J, Fales HM, Sokoloski EA, Levine RL, Vasquez-Vivar J, et al. (2005). Detection and characterization of the product of hydroethidine and intracellular superoxide by HPLC and limitations of fluorescence. Proceedings of the National Academy of Sciences of the United States of America, 102, 5727–5732 [Erratum: Proceedings of the National Academy of Sciences of the United States of America, 102, 9086, 2005.]. [PubMed: 15824309]

Zhao H, Kalivendi S, Zhang H, Joseph J, Nithipatikom K, Vasquez-Vivar J, et al. (2003). Superoxide reacts with hydroethidine but forms a fluorescent product that is distinctly different from ethidium:

Potential implications in intracellular fluorescence detection of superoxide. Free Radical Biology & Medicine, 34, 1359–1368. [PubMed: 12757846]

Zielonka J, & Kalyanaraman B (2010). Hydroethidine- and MitoSOX-derived red fluorescence is not a reliable indicator of intracellular superoxide formation: Another inconvenient truth. Free Radical Biology & Medicine, 48, 983–1001. [PubMed: 20116425]

Zielonka J, Sikora A, Hardy M, Joseph J, Dranka BP, & Kalyanaraman B (2012). Boronate probes as diagnostic tools for real time monitoring of peroxynitrite and hydroperoxides. Chemical Research in Toxicology, 25, 1793–1799. [PubMed: 22731669]

Zielonka J, Sikora A, Joseph J, & Kalyanaraman B (2010). Peroxynitrite is the major species formed from different flux ratios of co-generated nitric oxide and superoxide: Direct reaction with boronate-based fluorescent probe. Journal of Biological Chemistry, 285, 14210–14216. [PubMed: 20194496]

Zielonka J, Srinivasan S, Hardy M, Ouari O, Lopez M, Vasquez-Vivar J, et al. (2008). Cytochrome c-mediated oxidation of hydroethidine and mito-hydroethidine in mitochondria: Identification of homo- and heterodimers. Free Radical Biology & Medicine, 44, 835–846. [PubMed: 18155177]

Zielonka J, Vasquez-Vivar J, & Kalyanaraman B (2008). Detection of 2-hydroxyethidium in cellular systems: A unique marker product of superoxide and hydroethidine. Nature Protocols, 3, 8–21. [PubMed: 18193017]

Zielonka J, Zielonka M, Sikora A, Adamus J, Hardy M, Ouari O, et al. (2012). Global profiling of reactive oxygen and nitrogen species in biological systems: High-throughput real-time analyses. Journal of Biological Chemistry, 287, 2984–2995. [PubMed: 22139901]

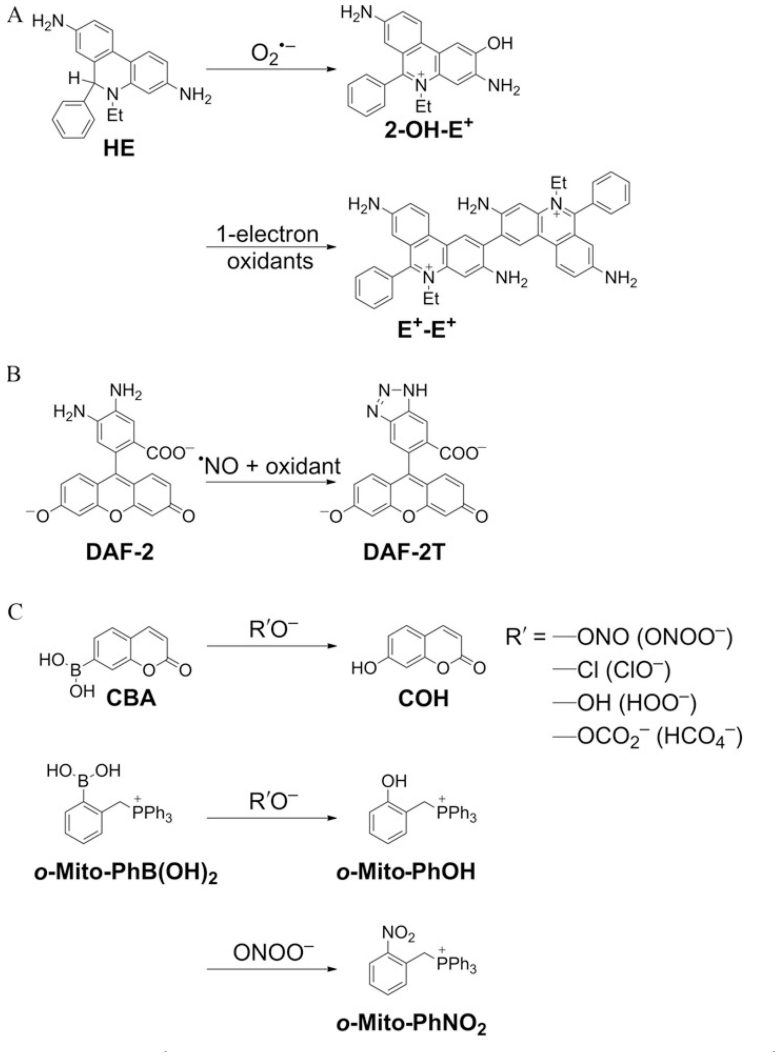

Figure 9.1.

Structures of chemical probes and their diagnostic marker products formed from reaction between (A) HE and superoxide or one-electron oxidants, (B) DAF-2 and nitric oxide and oxidant, and (C) CBA/o-Mito-PhB(OH)$_2$ and peroxy anion or peroxynitrite.

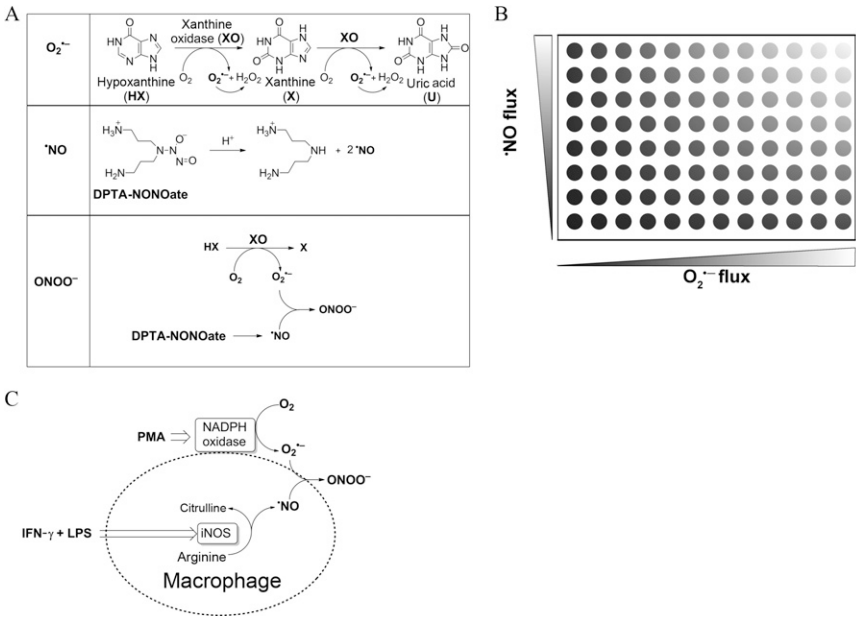

Figure 9.2.

(A) Peroxynitrite generation from cogenerated $O_2^{\bullet-}$ and $^{\bullet}NO$. Schemes showing formation of $O_2^{\bullet-}$ from incubations containing hypoxanthine (100 μ*M*) and xanthine oxidase (0–0.4 mU/ml) in a phosphate buffer (pH 7.4; 50 m*M*) containing dtpa (100 μ*M*), $^{\bullet}NO$ generation from a thermal decomposition of DPTA-NONOate (0–50 μ*M*), and $ONOO^-$ formed from cogenerated $O_2^{\bullet-}$from HX/XO and $^{\bullet}NO$ from DPTA-NONOate. (B) Diagrammatic representation of global profiling experiments. Varying fluxes of cogenerated $^{\bullet}NO$ and $O_2^{\bullet-}$ in a 96-well plate. The top right corner well represents conditions generating maximal (1:1) amount of $^{\bullet}NO$ and $O_2^{\bullet-}$ and bottom right corner well represents conditions generating maximal $O_2^{\bullet-}$ and H_2O_2 alone. (C) Reactive oxygen and nitrogen species formation from RAW 264.7 macrophages activated with LPS, IFN-γ, and PMA.

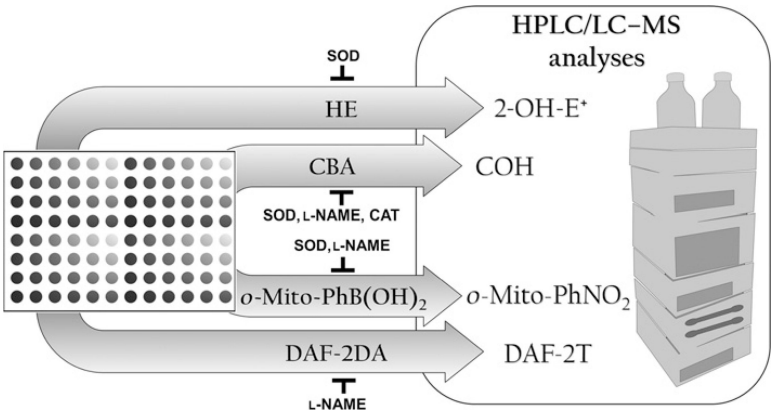

Figure 9.3.

Schematic representation of the proposed experimental approach for HPLC (or UHPLC)-based specific monitoring of superoxide (HE oxidation to 2-OH-E^+), nitric oxide (nitrosation of DAF-2 to DAF-2T), and peroxynitrite (oxidation of CBA to COH and transformation of o-Mito-$PhB(OH)_2$ to *o*-Mito-PhOH and *o*-Mito-$PhNO_2$). The identity of the species detected is confirmed by using specific inhibitors and/or scavengers. Rapid separation and detection with UHPLC systems enable analysis of samples in 96- or 384-well plate format.

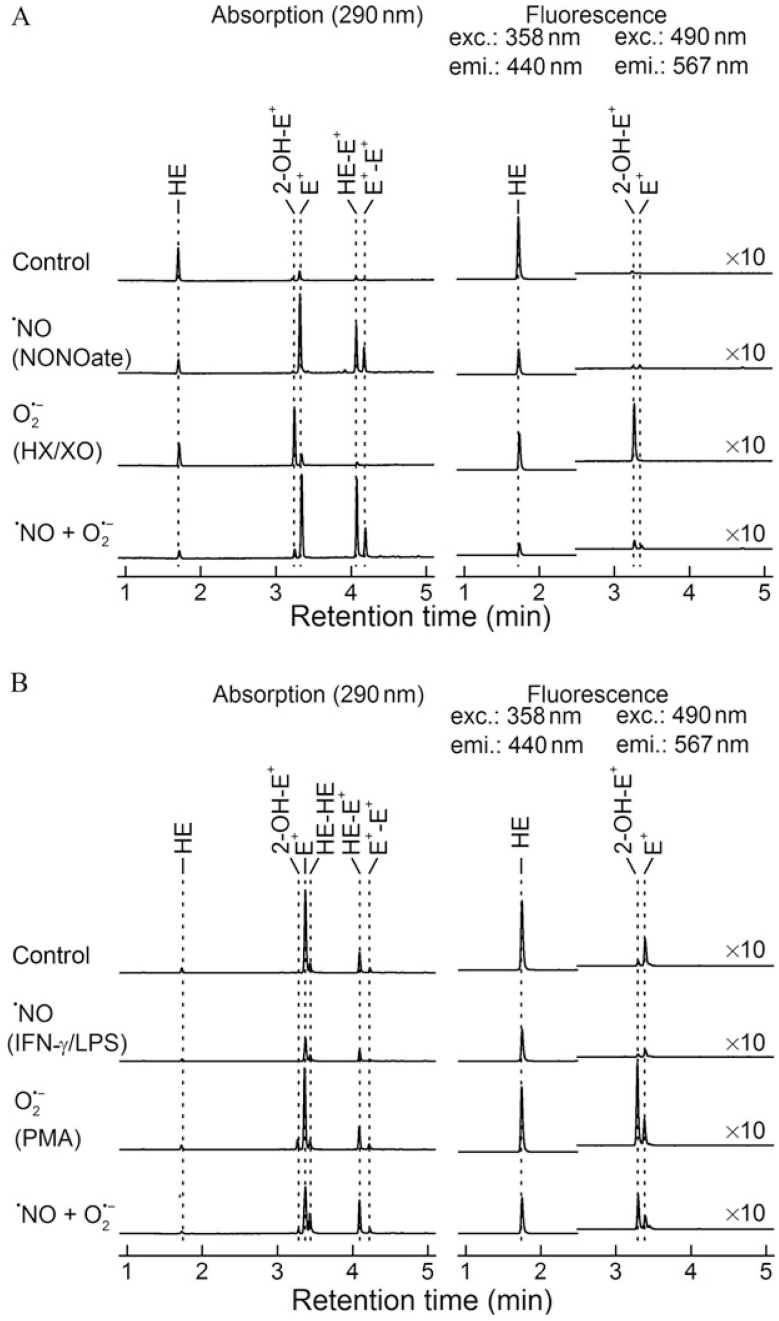

Figure 9.4.

Oxidation products formed from HE. (A) HPLC profiles of HE oxidation in cell- free incubations containing DPTA-NONOate alone, hypoxanthine and xanthine oxidase, and both DPTA-NONOate and hypoxanthine and xanthine oxidase, and (B) HPLC profiles obtained from cell lysates of RAW 264.7 macrophages stimulated to produce $^{\cdot}NO$, $O_2^{\cdot-}$, and both $^{\cdot}NO$ and $O_2^{\cdot-}$.

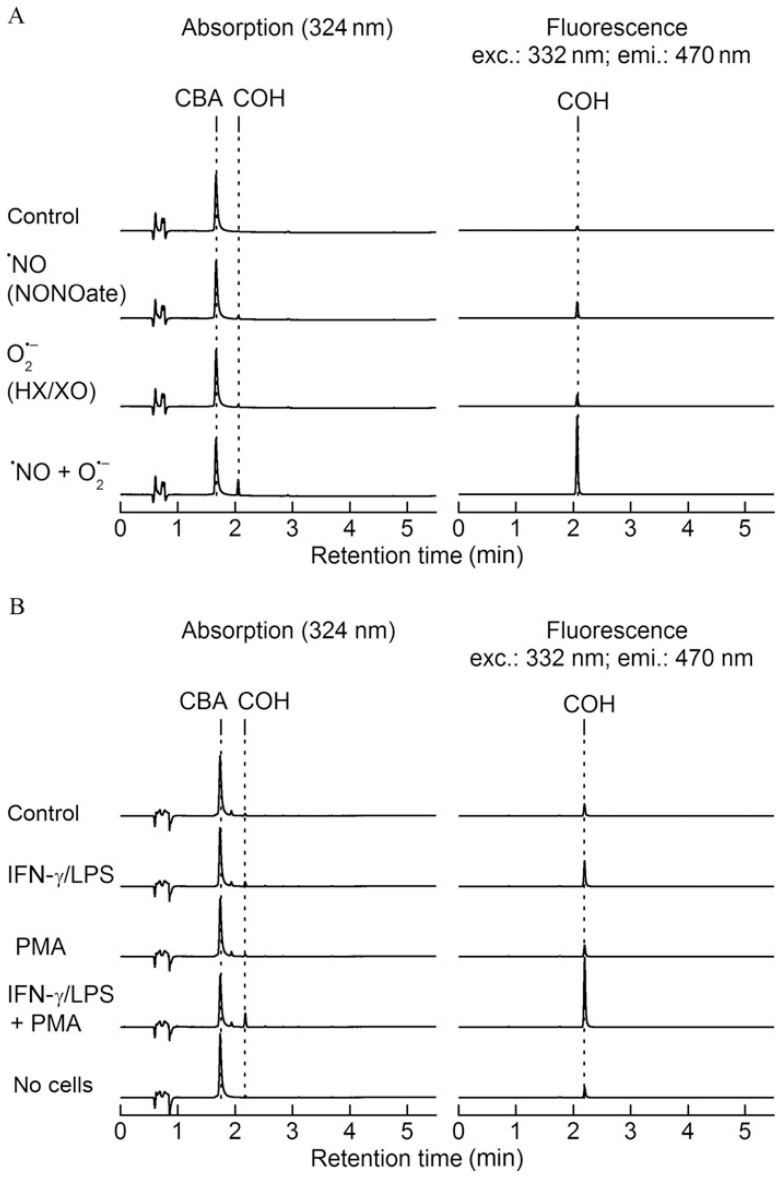

Figure 9.5.

Oxidation products formed from CBA. (A) HPLC profiles of CBA oxidation in cell-free incubations containing DPTA-NONOate alone, hypoxanthine and xanthine oxidase, and both DPTA-NONOate and hypoxanthine and xanthine oxidase, and (B) HPLC profiles obtained from cell media of RAW 264.7 macrophages stimulated to produce $^{\cdot}NO$, $O_2^{\cdot-}$, and both $^{\cdot}NO$ and O_2^{-}.

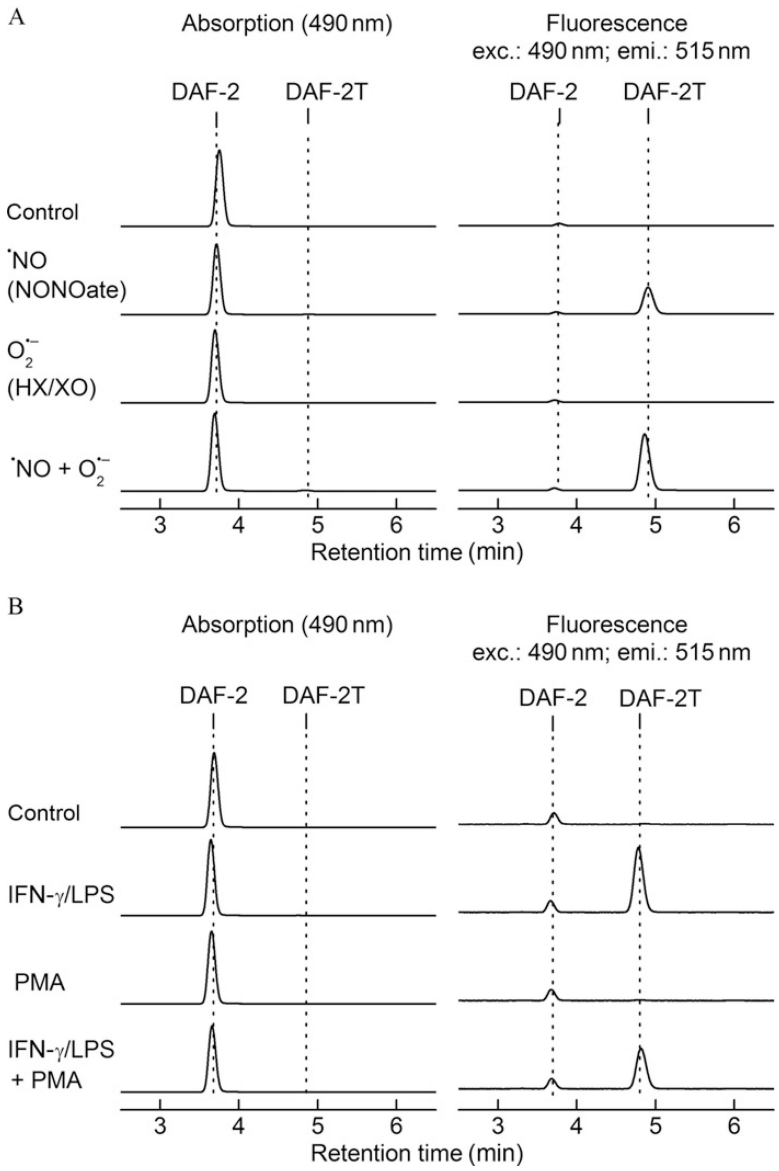

Figure 9.6.

HPLC profiles of DAF-2-derived products. (A) Nitrosation of DAF-2 (5 μ*M*) was monitored in a “cell-free” system. As shown, ·NO is required to form the specific nitrosated product, DAF-2T. (B) Nitrosation of DAF-2 (5 μ*M*) in media of activated RAW 264.7 macrophages.

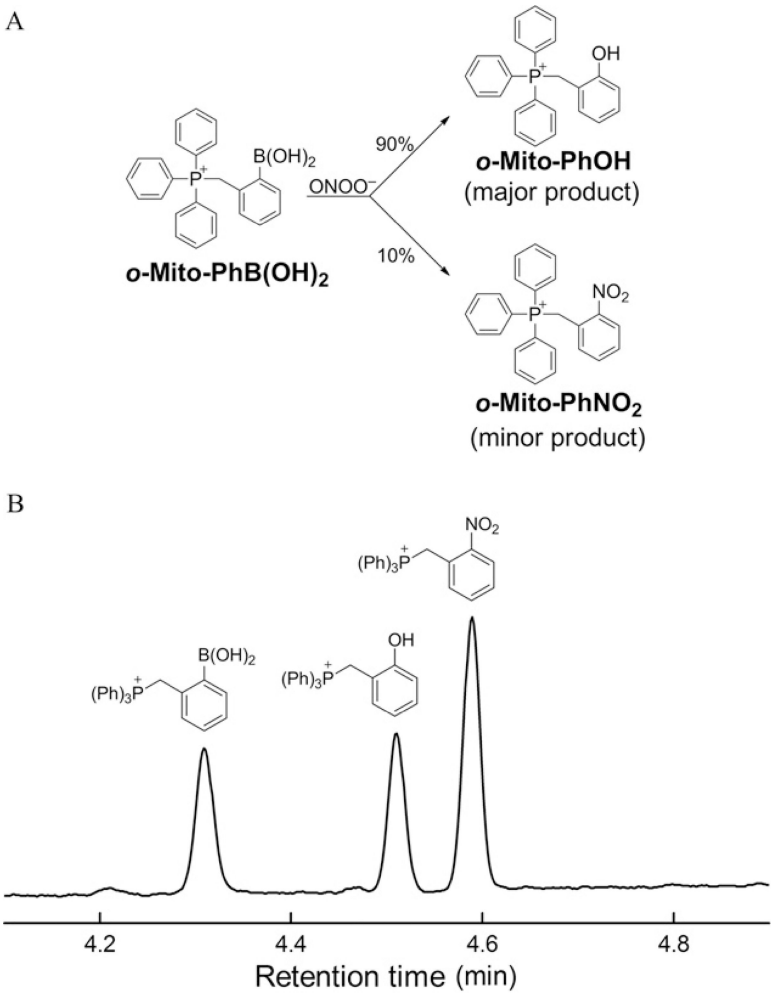

Figure 9.7.

HPLC profiles of *o*-Mito-PhB(OH)$_2$-derived products. (A) Scheme showing the major (*o*-Mito-PhOH) and minor (*o*-Mito-PhNO$_2$) products of the reaction of *o*-Mito-PhB(OH)$_2$ with $ONOO^-$. (B) HPLC chromatogram of the standards of *o*-Mito- PhB(OH)$_2$, *o*-Mito-PhOH and *o*-Mito-PhNO$_2$.